



## PEG-PLA nanoparticles modified with APT<sub>EDB</sub> peptide for enhanced anti-angiogenic and anti-glioma therapy



Guangzhi Gu<sup>a, c, 1</sup>, Quanyin Hu<sup>a, 1</sup>, Xingye Feng<sup>a</sup>, Xiaoling Gao<sup>b</sup>, Jiang Menglin<sup>a</sup>, Ting Kang<sup>a</sup>, Di Jiang<sup>a</sup>, Qingxiang Song<sup>b</sup>, Hongzhuan Chen<sup>b</sup>, Jun Chen<sup>a, \*</sup>

<sup>a</sup> Key Laboratory of Smart Drug Delivery, Ministry of Education, School of Pharmacy, Fudan University, Lane 826, Zhangheng Road, Shanghai 201203, PR China

<sup>b</sup> Department of Pharmacology, Institute of Medical Sciences, Shanghai Jiaotong University School of Medicine, 280 South Chongqing Road, Shanghai 200025, PR China

<sup>c</sup> Shanghai Institute for Food and Drug Control (SIFDC), 479 Futexi First Road, Shanghai 200131, PR China

### ARTICLE INFO

#### Article history:

Received 23 May 2014

Accepted 9 June 2014

Available online 25 June 2014

#### Keywords:

Nanoparticles  
APTEDB peptide  
Dual-targeting  
Paclitaxel  
Glioma therapy

### ABSTRACT

Tumor neovasculature and tumor cells dual-targeting chemotherapy can not only destroy the tumor neovasculature, cut off the supply of nutrition and starve the tumor cells, but also directly kill tumor cells, holding great potential in overcoming the drawbacks of anti-angiogenic therapy only and improving the anti-glioma efficacy. In the present study, by taking advantage of the specific expression of fibronectin extra domain B (EDB) on both glioma neovasculature endothelial cells and glioma cells, we constructed EDB-targeted peptide APT<sub>EDB</sub>-modified PEG-PLA nanoparticles (APT-NP) for paclitaxel (PTX) loading to enable tumor neovasculature and tumor cells dual-targeting chemotherapy. PTX-loaded APT-NP showed satisfactory encapsulated efficiency, loading capacity and size distribution. In human umbilical vein endothelial cells, APT-NP exhibited significantly elevated cellular accumulation via energy-dependent, caveolae and lipid raft-involved endocytosis, and improved PTX-induced apoptosis therein. Both *in vitro* tube formation assay and *in vivo* matrigel angiogenesis analysis confirmed that APT-NP significantly improved the antiangiogenic ability of PTX. In U87MG cells, APT-NP showed elevated cellular internalization and also enhanced the cytotoxicity of the loaded PTX. Following intravenous administration, as shown by both *in vivo* live animal imaging and tissue distribution analysis, APT-NP achieved a much higher and specific accumulation within the glioma. As a result, APT-NP-PTX exhibited improved anti-glioma efficacy over unmodified nanoparticles and Taxol<sup>®</sup> in both subcutaneous and intracranial U87MG xenograft models. These findings collectively indicated that APT<sub>EDB</sub>-modified nanoparticles might serve as a promising nanocarrier for tumor cells and neovasculature dual-targeting chemotherapy and hold great potential in improving the efficacy anti-glioma therapy.

© 2014 Elsevier Ltd. All rights reserved.

### 1. Introduction

Glioma stands out as one of the world's most devastating diseases, with a 5-year survival rate of less than 10% [1]. Although the combination of surgery, radiotherapy and chemotherapy are capable of treating glioma in clinic now, improvements in treatment outcomes are modest [2,3]. Chemotherapy has been considered as the most common auxiliary treatment for glioma, while the poor efficiency of drug delivery to glioma significantly restricts its

application due to non-targeted nature of anti-cancer drugs and several physiologic barriers including blood–brain barrier (BBB) and blood-tumor barrier (BTB) [4].

Angiogenesis, the sprouting of new blood vessels from existing parent ones, is a crucial event for tumor growth, evasion and metastasis [5]. Gliomas are highly vascular and rich in VEGF, which promotes angiogenesis [6]. Anti-angiogenesis therapy has come to the forefront as an alternative to other glioma treatment strategies including bypassing the BBB/BTB and targeting drugs directly to the glioma tissue not only because endothelial cells are more easily accessible [7,8], but also because endothelial cells have an intrinsic amplification mechanism which means damaging a single vessel can potentially have an impact on the growth of a large number of tumor cells [9].

\* Corresponding author. Tel.: +86 21 51980066.

E-mail addresses: [chenjun@fudan.edu.cn](mailto:chenjun@fudan.edu.cn), [chenjun\\_1974@aliyun.com](mailto:chenjun_1974@aliyun.com) (J. Chen).

<sup>1</sup> Authors contributed equally.

However, current evidences indicates that anti-angiogenic therapy only also associates with a series of adverse effects, such as intrinsic/acquired anti-angiogenic drug resistance and increased local invasion or distant metastasis, and even tumor recurrence [10]. Tumor neovasculature and tumor cells dual-targeting chemotherapy offers an alternative option and might provide a more promising therapeutic strategy as it can not only destroy the tumor neovasculature, cut off the supply of nutrition and starve the tumor cells, but also directly kill tumor cells [11,12], holding great potential in reducing the unwanted side effect after anti-angiogenic therapy only.

Effective tumor neovasculature and tumor cells dual-targeting relies on the identification of high-quality biomarkers of pathology [13]. One well-characterized marker is fibronectin extra domain B (EDB), a 91-amino-acid type III homology domain identical in mice, rats, rabbit, dog, monkey, and humans, which can be inserted into the fibronectin molecule by a mechanism of alternative splicing [14]. EDB-containing fibronectin is abundant in many aggressive solid tumors [15,16]. More importantly, EDB is selectively expressed in tumor-associated blood vessels and tumor extracellular matrix but virtually undetectable in normal adult tissues (except in regenerating endometrium), and its expression level is very often positively correlated with the grade of tumor malignancy [17,18]. Therefore, targeting the EDB may provide an opportunity to selective and effective delivery of chemotherapeutics-loaded nanoparticles to tumor site without causing harmful effects on normal tissue.

APT<sub>EDB</sub>, a small aptamer-like peptide (aptide) with 26 amino acids, is identified via phage display and possesses high affinity and specificity to EDB at nanomolar level [19]. It was showed that APT<sub>EDB</sub> specifically stained EDB protein in the *ex vivo* tumor tissue in a manner similar to anti-EDB antibody. As high binding affinity is desirable for achieving an efficient tumor neovasculature and tumor cells dual-targeting [20,21], we believe that APT<sub>EDB</sub> holds great potential for being utilized as a promising ligand for anti-angiogenic and anti-glioma therapy.

In this study, encapsulating paclitaxel (PTX) as the model drug, tumor vasculature and tumor cells dual-targeted PEG-PLA nanoparticles were constructed by conjugating APT<sub>EDB</sub> ligand on the particle surface, aiming at improving the drug's anti-angiogenic and anti-glioma efficacy. Cellular uptake of the functionalized nanoparticles and the mechanism of cellular internalization were investigated in both HUVEC and U87MG cells. *In vitro* tube formation assay and *in vivo* matrigel angiogenesis assay were performed to confirm the anti-angiogenic activity of APT-NP-PTX. The *in vivo* tumor targeting and anti-glioma efficacy of APT-NP-PTX were evaluated in U87MG tumor xenograft model.

## 2. Materials and methods

### 2.1. Materials

APT<sub>EDB</sub> (SSSPIQGSWTWENGKGCWTWKGIIRLEQ) was synthesized by ChinaPeptides Co., Ltd (Shanghai, China). Methoxy poly (ethylene glycol) 3000-poly (lactic acid) 34000 (MePEG-PLA) and maleimide-poly (ethylene glycol) 3400-poly (lactic acid) 34000 (Male-PEG-PLA) were kindly provided by East China University of Science and Technology. Paclitaxel was purchased from Xi'an Sanjiang Bio-Engineering Co. Ltd. (Xi'an, China) and Taxol<sup>®</sup> from Bristol-Myers Squibb Company. Recombinant human basic fibroblast growth factor (bFGF), growth factor-reduced Matrigel matrix and Annexin V-FITC Apoptosis Detection Kit 1 were purchased from BD Biosciences (San Diego, CA, USA). Cell counting kit-8 (CCK-8) was provided Dojindo (Kumamoto, Japan) and Alexa Fluor<sup>®</sup> 647 anti-mouse CD31 Antibody was obtained from BioLegend (San Diego, CA, USA). Hoechst 33258 and Coumarin-6 were obtained from Sigma-Aldrich (St. Louis, MO, USA), and 4,6-diamidino-2-phenylindole (DAPI) from Molecular Probes (Eugene, OR, USA). 1, 1'-dioctadecyl-3, 3', 3', 3'-tetramethyl indotricarbocyanine Iodide (DiR) was purchased from Biotium (Hayward, CA). All the other solvents were analytical or chromatographic grade.

Primary human umbilical vein endothelial cells (HUVEC) were purchased from Cascade Biologics (USA) and grown in Medium 200 (M200, Cascade Biologics, USA)

supplemented with low serum growth supplement (LSGS) at 37 °C in a humidified atmosphere containing 5% CO<sub>2</sub>. U87MG glioblastoma cell was obtained from Cell Institute of Chinese Academy of Sciences (Shanghai, China) and maintained in DMEM supplemented with containing 10% FBS, 100 U/ml penicillin and 100 mg/ml streptomycin at 37 °C in a humidified atmosphere containing 5% CO<sub>2</sub>.

Male BALB/c nude mice (20 ± 2 g) were purchased from the BK Lab Animal Ltd (Shanghai, China) and maintained at 25 ± 1 °C with free access to food and water. All the animal experiments were carried out in accordance with guidelines evaluated and approved by the ethics committee of Fudan University (Shanghai, China).

### 2.2. Preparation of nanoparticles

PEG-PLA nanoparticles (NP) loaded with PTX were prepared with a blend of MePEG-PLA and Male-PEG-PLA using the emulsion/solvent evaporation technique according to the procedure described elsewhere [22]. In brief, MePEG-PLA (22.5 mg), Male-PEG-PLA (2.5 mg) and PTX (0.5 mg) were dissolved in 1 mL of dichloromethane, followed by the addition of 2 mL of 1% sodium cholate, emulsified by sonication (280 W, 30 s) on ice using probe sonicator (Ningbo Scientz Biotechnology Co. Ltd., China). The resulted O/W emulsion was further diluted into a 10 mL of 0.5% sodium cholate aqueous solution under rapid magnetic stirring for 5 min and dichloromethane was rapidly eliminated by evaporation under vacuum. The formed NP was collected by centrifugation at 14,500 rpm using a TJ-25 centrifuge (Beckman Counter, USA) at 4 °C for 1 h and resuspended in 1 mL 0.01 M HEPES buffer (pH 7.0).

The preparation of fluorescein-labeled nanoparticles was prepared with the same procedure except 25 µg coumarin-6 or 0.25 mg DiR were dissolved in the dichloromethane solution.

Nanoparticles modified with APT<sub>EDB</sub> (APT-NP) were prepared via a maleimide-thiol coupling reaction at room temperature for 8 h as described previously [23,24]. The products were then eluted with 0.01 M HEPES buffer (pH 7.0) through a 1.5 × 20 cm sepharose CL-4B column to remove the unconjugated peptide.

### 2.3. Characterization of nanoparticles

#### 2.3.1. Particle size distribution, zeta potential and morphology

Particle size and zeta potential of PTX-loaded PEG-PLA nanoparticles (NP-PTX) and APT<sub>EDB</sub> peptide-conjugated PTX-loaded PEG-PLA nanoparticles (APT-NP-PTX) were determined using a Malvern Zeta Sizer Nano series (Malvern Instruments, Worcestershire, UK). The morphological examination of nanoparticles was carried out by transmission electron microscope (H-600, Hitachi, Japan).

#### 2.3.2. X-ray photo electron spectroscopy (XPS)

To verify the modification with APT<sub>EDB</sub> peptide, the nanoparticle samples were lyophilized using an ALPHA 2-4 Freeze Dryer (0.070 Mbar Vacuum, -80 °C, Martin Christ, Germany) and subjected to XPS analysis on a RBD upgraded PHI-5000C ESCA system (Perkin Elmer) to determine the surface composition of C, O and N.

#### 2.3.3. Encapsulation efficiency (EE) and loading capacity (LC)

The encapsulation efficiency (EE) and loading capacity (LC) of PTX in NP-PTX and APT-NP-PTX were determined by high performance liquid chromatography (HPLC) as described previously [25].

The EE% and LC% were calculated as indicated below:

$$EE(\%) = \frac{\text{Amount of PTX in the nanoparticles}}{\text{Total amount of PTX added}} \times 100\%$$

$$LC(\%) = \frac{\text{Amount of PTX in nanoparticles}}{\text{Weight of nanoparticles}} \times 100\%$$

#### 2.3.4. *In vitro* PTX release

*In vitro* PTX release from both NP-PTX and APT-NP-PTX was performed as described previously using phosphate buffer solution (PBS, pH 7.4) containing 0.5% (V/V) Tween-80 and 10% rat plasma as the media, respectively [26]. Briefly, 1 mL of the PTX formulation (containing 80 µg PTX) was introduced into a dialysis bag (MWCO = 8000 Da, Greenbird Inc., Shanghai, China), which was then immersed in 39 mL release medium and incubated at 37 °C at the shaking speed of 120 rpm for 96 h. At predetermined time points, 200 µL of sample was withdrawn and the concentration of PTX was analyzed by HPLC as described previously [27].

### 2.4. Cellular association of coumarin-6-labeled nanoparticles in HUVEC and U87MG cells

HUVEC cells and U87MG cells were seeded in 96-well plates at the density of 5000 cells/well. For qualitative experiment, on the second day, the cells were incubated with coumarin-6-labeled NP and APT-NP in serum-free media for 1 h at different concentrations ranging from 50 to 400 µg/mL, respectively, at 37 °C. After that, the cells were washed three times with PBS, fixed with 4% paraformaldehyde for 15 min and then subjected to fluorescent microscopy analysis (Leica DMI4000 B, Germany).

For quantitative experiment, HUVEC cells and U87MG were incubated with NP and APT-NP (50–400  $\mu\text{g}/\text{ml}$ ) for 1 h at 4 °C and 37 °C, respectively. In order to study the effects of incubation time on nanoparticle uptake, HUVEC cells and U87MG cells were incubated with 200  $\mu\text{g}/\text{ml}$  nanoparticles for 30 min, 1 h, 2 h and 4 h at 37 °C, respectively, in a separate experiment. Thereafter, the cells were washed with PBS and fixed with 4% paraformaldehyde solution for 15 min. After stained with 2  $\mu\text{g}/\text{ml}$  Hoechst 33258 at room temperature for 10 min, away from light, the cells were finally washed with PBS for three times and detected under a KineticScan<sup>®</sup> HCS Reader (version 3.1, Cellomics Inc., Pittsburgh, PA, USA).

### 2.5. Mechanism of cellular internalization of APT-NP

Endocytosis inhibition experiments were performed to investigate the cellular internalization mechanism for APT-NP in HUVEC cells. HUVEC cells were seeded in a 96-well plate at the density of 5000 cells/well and cultured for 24 h. Prior to incubation with APT-NP (200  $\mu\text{g}/\text{ml}$ , 1 h, 37 °C), the cells were preincubated with endocytic inhibitors including 10  $\mu\text{g}/\text{ml}$  chlorpromazine, 4  $\mu\text{g}/\text{ml}$  colchicines, 10  $\mu\text{g}/\text{ml}$  cyto-D, 5  $\mu\text{g}/\text{ml}$  BFA, 5  $\mu\text{g}/\text{ml}$  filipin, 2.5  $\mu\text{g}/\text{ml}$  genistein, 10 mM  $\text{Na}_3\text{N}$  + 50 mM deoxyglucose, 2.5 mM methyl- $\beta$ -cyclodextrin (M- $\beta$ -CD), 200 nM monensin, 20  $\mu\text{M}$  nocodazole and 200  $\mu\text{g}/\text{ml}$  APT<sub>EDB</sub> peptide were incubated with the cells for 1 h. After that, quantitative analysis was performed as described above.

### 2.6. Cell apoptosis assay

HUVEC cells were seeded in 6-well plates at the density of  $5 \times 10^5$  cells per well and cultured at 37 °C for 24 h. Cells were then incubated for another 24 h with Taxol<sup>®</sup>, NP-PTX and APT-NP-PTX (PTX concentration of 100 ng/ml) and culture medium as control. Thereafter, the cells were fixed with 4% paraformaldehyde for 15 min, stained with 10  $\mu\text{g}/\text{ml}$  Hoechst 33528 at room temperature for 15 min, washed twice with ice-cold PBS. Finally, the nuclear morphology was checked using a fluorescent microscope (Leica DMI4000 B, Germany).

For quantitative analysis, cells were left untreated or were treated with Taxol<sup>®</sup>, NP-PTX and APT-NP-PTX (PTX concentration of 100 ng/ml) for 24 h. Then, non-adherent and adherent cells were trypsinized with trypsin and centrifuged with the pellet re-suspended in 200  $\mu\text{l}$  of binding buffer for double staining with Annexin V-FITC (5  $\mu\text{l}$ ) and PI (10  $\mu\text{l}$ ) according to the manufacturer's protocol. The stained cells were analyzed using a flow cytometer (FACSCalibur, BD, USA). Data analysis was performed using Cell-Quest software (Becton Dickinson, USA).

### 2.7. In vitro tube formation assay

Prechilled 96-well plate were coated with 50  $\mu\text{l}$  growth factor-reduced Matrigel and incubated at 37 °C for 1 h to allow the Matrigel to polymerize [28]. HUVEC cells were trypsinized, resuspended in M200 medium supplemented with LSGS containing different concentrations of paclitaxel (1, 5 and 10 nM) and then seeded onto the Matrigel at a density of  $2 \times 10^4$  cells/well. The medium containing no paclitaxel was set as controls. After being shaken for 15 s with orbital shaker, the plate was kept in the cell incubator for 8 h. Then, branches of capillary-like tube were

examined and photographed using a phase-contrast microscopy ( $\times 40$  magnification) and counted for statistical analysis ( $n = 3$ ).

### 2.8. In vivo matrigel angiogenesis assay

Two-month-old BALB/c nude mice were injected in the abdominal region with 200  $\mu\text{l}$  growth factor-reduced Matrigel containing 200 ng of human recombinant bFGF as an angiogenesis stimulant [29]. The mice were treated with daily i.v. injections of 200  $\mu\text{l}$  Taxol<sup>®</sup>, NP-PTX and APT-NP-PTX (at a dose of 5 mg/kg PTX), or physiological saline as a control for 7 days. Each treatment group consisted of a minimum of three mice. At the end of treatment, Matrigel plugs were removed, fixed in 4% paraformaldehyde, cryoprotected in sucrose solution, and subjected to OCT embedding and frozen section. Thereafter, the slides were stained by immunofluorescence with anti-CD31 to show the blood vessels: the frozen slices firstly blocked with 20% goat serum for 1 h at room temperature, and then incubated with Alexa Fluor<sup>®</sup> 647 anti-mouse CD31 antibody ( $1 \times 100$  dilution) overnight at 4 °C. Finally, the slides were treated with DAPI for nuclear counterstain, and visualized under a Zeiss LSM 510 confocal microscope.

### 2.9. Anti-proliferation assay

U87MG cells were seeded into 96-well plates at the density of 5000 cells/well and incubated for 24 h at 37 °C in a 5%  $\text{CO}_2$  atmosphere to allow cell attachment. After that, the medium was refreshed with 200  $\mu\text{l}$  serum-free medium containing Taxol<sup>®</sup>, NP-PTX and APT-NP-PTX, respectively, at the PTX concentrations ranging from 1 ng to 10  $\mu\text{g}$ . Cells without exposure to the PTX formulations were used as control. After 72 h incubation, cell viability was evaluated via Cell Counting Kit-8 (CCK-8) assay according to the manufacturer's instruction.

### 2.10. In vivo imaging

The subcutaneous tumor xenograft model was established by inoculation of  $5 \times 10^6$  U87MG cells (in 200  $\mu\text{l}$  cell culture medium) into the subcutaneous tissue of the armpit of right anterior limb [30]. When the size of tumors reached 0.6–0.8 cm in diameter, the tumor-bearing mice were injected with 200  $\mu\text{l}$  DiR-loaded NP or APT-NP (1 mg/kg). The fluorescent images were acquired at 2, 6, 12 and 24 h after injection using a CRI *in vivo* imaging system (CRI, MA, USA). After 24 h post-injection, the mice were sacrificed with the tumor and principle organs (including heart, liver, spleen, lung and kidney) harvested and visualized under the CRI *in vitro* imaging system.

### 2.11. In vivo tumor distribution

The subcutaneous U87MG tumor-bearing mice were injected intravenously with coumarin-6-loaded NP and APT-NP, respectively, at the equal dose of coumarin-6. After 3 h of circulation, the mice were anesthetized, and heart perfused with saline and 4% paraformaldehyde, followed by preparation of 10  $\mu\text{m}$  sections from the tumors. Following the same procedure described in 2.8, the sections were stained by immunofluorescence with anti-CD31 for tumor blood vessel and DAPI

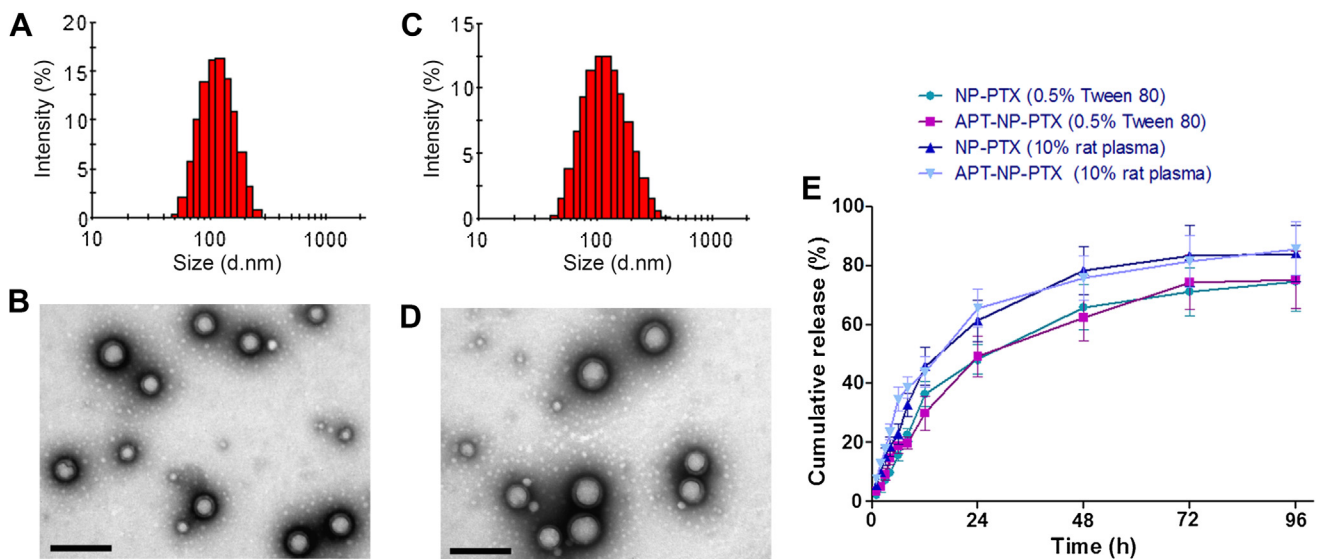


**Fig. 1.** Characterization of NP-PTX and APT-NP-PTX. Particle size distribution and TEM image of NP-PTX (A, B) and APT-NP-PTX (C, D). PTX release profiles from NP-PTX and APT-NP-PTX in PBS (pH 7.4) with 0.5% Tween-80 and PBS (pH 7.4) containing 10% rat plasma at 37 °C (E). The bar is 200 nm.

**Table 1**  
Physical characterization of NP-PTX and APT-NP-PTX (Data represent mean  $\pm$  SD,  $n = 3$ ).

Nanoparticles	Mean size (mean $\pm$ SD, nm)	Polydispersity index (P.I.)	Zeta potential (mV)
NP-PTX	112.80 $\pm$ 5.05	0.11 $\pm$ 0.04	-35.50 $\pm$ 1.11
APT-NP-PTX	125.93 $\pm$ 9.84	0.19 $\pm$ 0.03	-30.87 $\pm$ 2.46

was used for nuclei staining. Finally, the sections were examined under a Zeiss LSM 510 confocal microscope.

#### 2.12. *In vivo* antitumor activity evaluation

The subcutaneous tumor xenograft model was established as demonstrated in 2.9 and used for tumor growth inhibition experiment. The dose schedule started when the tumor volume reached about 50–70 mm<sup>3</sup>. The mice were randomly assigned to four groups ( $n = 6$ ) to receive 200  $\mu$ l of Taxol<sup>®</sup>, NP-PTX, APT-NP-PTX (PTX dose of 5 mg/kg) and physiological saline via tail vein injection. The treatment was repeated every three days for five consecutive injections. Tumor size was monitored every other day via serial caliper measurement and the tumor volume was estimated using the formula: Volume =  $\pi/6 \times$  larger diameter  $\times$  (smaller diameter)<sup>2</sup>. At the end of the experiment, mice were sacrificed by cervical dislocation, and the tumor masses were harvested and then weighed.

#### 2.13. Anti-glioma effect

Twenty-four nude mice bearing intracranial U87MG glioma were divided into four groups randomly ( $n = 6$ ), intravenously treated with Taxol<sup>®</sup>, NP-PTX and APT-

NP-PTX (PTX concentration of 5 mg/kg) and saline, respectively, at every three days in two weeks. The survival time of each group was recorded and analyzed.

#### 2.14. Statistical analysis

All the data were presented as mean  $\pm$  SD unless otherwise indicated. Comparison among the different groups was performed by one-way ANOVA followed by Bonferroni tests. And  $p < 0.05$  was considered significant.

### 3. Results

#### 3.1. Characterization of nanoparticles

The mean diameter of NP-PTX was 112.80  $\pm$  5.05 nm, while a slight increase in diameter was observed following its modification with APT<sub>EDB</sub> peptide (125.93  $\pm$  9.84 nm) (Fig. 1A, B). Representative TEM photographs illustrated that NP-PTX and APT-NP-PTX were both generally spherical (Fig. 1C, D). After modification, the zeta potential of NP-PTX (-35.50  $\pm$  1.11 mV) was slightly lower than that of APT-NP-PTX (-30.87  $\pm$  2.46 mV) (Table 1). The existence of APT<sub>EDB</sub> on the surface of APT-NP-PTX was confirmed by XPS analysis which showed that the elemental composition percentage of nitrogen on the surface of unmodified NP was undetectable, while that on the surface of APT-NP was 0.87%.

From our experiments, the EE of the optimized NP-PTX and APT-NP-PTX was 43.07  $\pm$  3.97% and 41.53  $\pm$  2.15%, respectively, with the LC 1.33  $\pm$  0.16% and 1.27  $\pm$  0.12%, respectively.

*In vitro* release experiment showed that NP-PTX and APT-NP-PTX exhibited similar release patterns in both release media

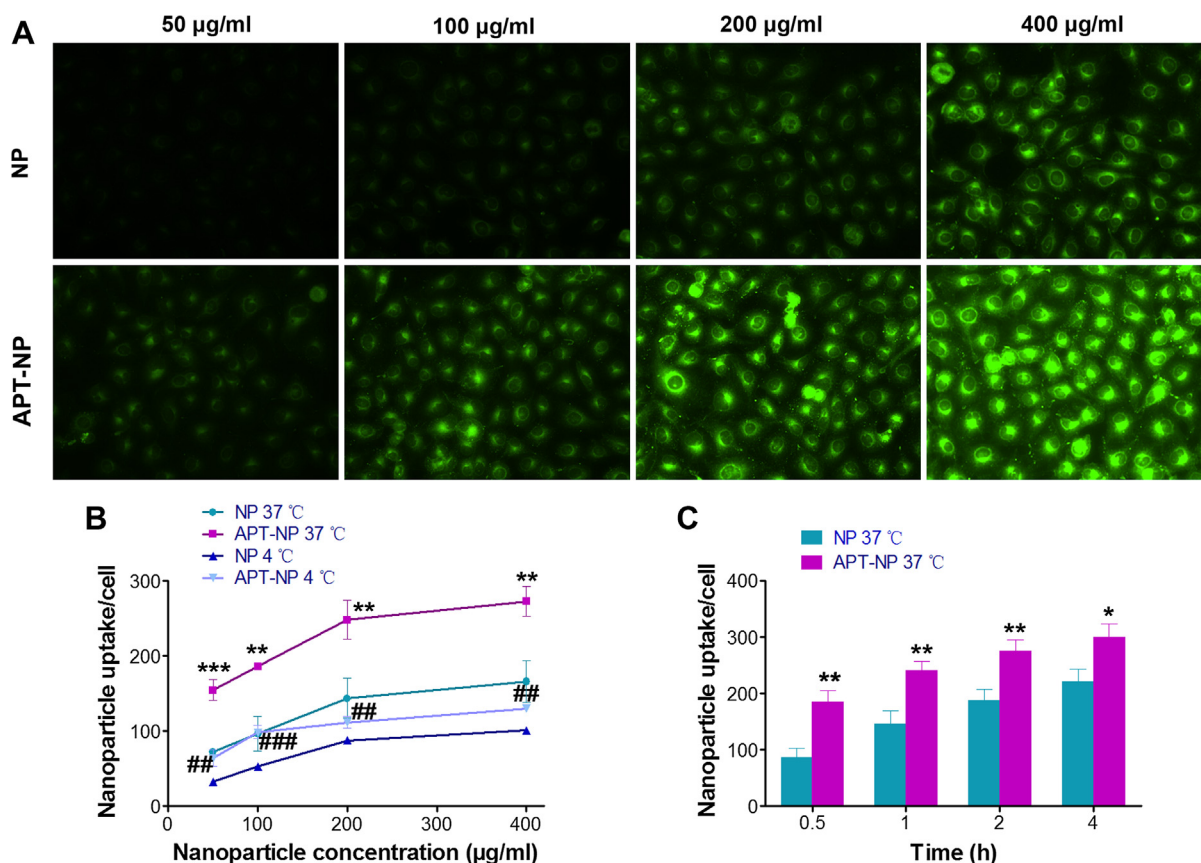


**Fig. 2.** (A) *In vitro* cellular association coumarin-6-labeled NP and APT-NP after 1 h incubation at 37 °C at different concentrations: 50  $\mu$ g/ml, 100  $\mu$ g/ml, 200  $\mu$ g/ml, 400  $\mu$ g/ml, respectively. Original magnification: 20 $\times$ . (B) Quantitative cellular association of NP and APT-NP in HUVEC cells after 1 h incubation with different concentrations of coumarin-6-labeled nanoparticles (from 50  $\mu$ g/ml to 400  $\mu$ g/ml) at 37 °C and 4 °C. (C) Quantitative cellular association of NP and APT-NP in HUVEC cells after incubation for 0.5 h–4 h at the NPs concentration of 200  $\mu$ g/ml. Data presented as mean  $\pm$  SD ( $n = 3$ ). \* $p < 0.05$ , \*\* $p < 0.01$ , \*\*\* $p < 0.001$  significantly higher than the cellular association of unmodified NP at 37 °C, and # $p < 0.05$ , ## $p < 0.01$ , ### $p < 0.001$  significantly higher than the cellular association of unmodified NP at 4 °C.

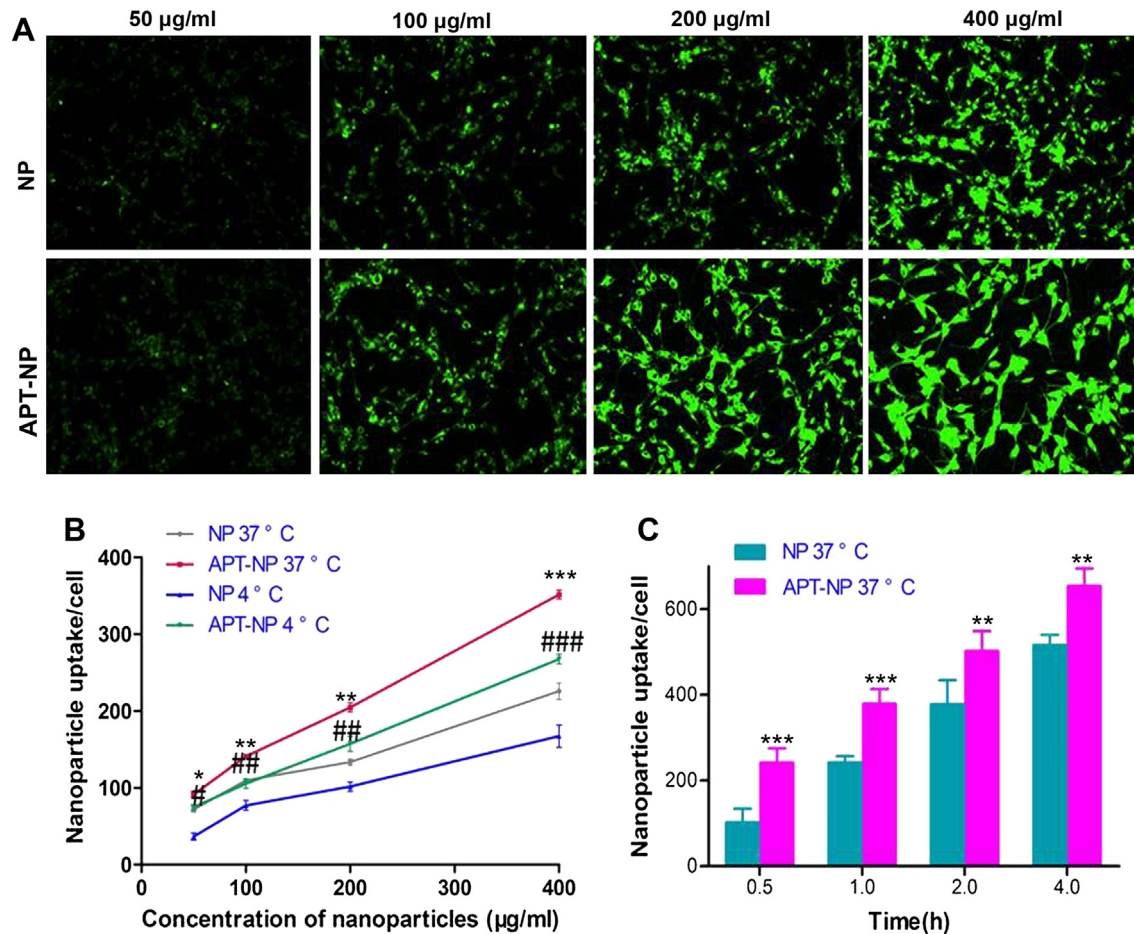


**Fig. 3.** (A) *In vitro* cellular association of coumarin-6-labeled NP and APT-NP in U87MG cells after 1 h incubation at 37 °C at different concentrations: 50 µg/ml, 100 µg/ml, 200 µg/ml, 400 µg/ml, respectively. Original magnification: 20×. (B) Quantitative cellular association of NP and APT-NP in U87MG cells after 1 h incubation with different concentrations of coumarin-6-labeled nanoparticles (from 50 µg/ml to 400 µg/ml) at 37 °C and 4 °C. (C) Quantitative cellular association of NP and APT-NP in U87MG cells after incubation for 0.5 h–4 h at the NPs concentration of 200 µg/ml. Data presented as mean ± SD ( $n = 3$ ). \* $p < 0.05$ , \*\* $p < 0.01$ , \*\*\* $p < 0.001$  significantly higher than the cellular association of unmodified NP at 37 °C, and # $p < 0.05$ , ## $p < 0.01$ , ### $p < 0.001$  significantly higher than the cellular association of unmodified NP at 4 °C.

(Fig. 1E). It was found that 76.43% of PTX in NP-PTX and 75.12% of PTX in APT-NP-PTX were released after 96 h incubation in PBS (pH 7.4), while 84.21% of PTX in NP-PTX and 85.75% of PTX in APT-NP-PTX were released in PBS (pH 7.4) containing 10% rat plasma, after 96 h incubation. A faster release pattern of nanoparticles in PBS (pH 7.4) containing 10% rat plasma was observed when compared with that in PBS (pH 7.4).

### 3.2. Cellular association in HUVEC cells and U87MG cells

Qualitative fluorescent microscopy analysis showed that HUVEC cells and U87MG treated with either coumarin-6-labeled NP or APT-NP exhibited fluorescent intensity corresponding to nanoparticle concentration. The cellular associated fluorescence intensity for APT-NP was significantly higher than that of NP at all the detected concentrations (Figs. 2A and 3A).

Quantitative high content analysis system analysis revealed the time-dependent, temperature-dependent and concentration-dependent mode of cellular uptake of APT-NP in HUVEC cells and U87MG cells (Fig. 2B, C, Fig. 3B, C). The cellular association of APT-NP was significantly higher than that of unmodified NP at the concentrations ranged from 50 µg/ml to 400 µg/ml and after the incubation time ranged from 0.5 h to 4 h. Furthermore, both NP and APT-NP exhibited much higher cellular associations at 37 °C than 4 °C.

### 3.3. Mechanism of cellular internalization of APT-NP

Inhibition experiment showed that the cellular uptake of APT-NP was significantly inhibited by Golgi apparatus destroyer – BFA, energy-depletion agent – NaN<sub>3</sub> and lipid raft inhibitor – M-β-CD ( $p < 0.05$ ,  $p < 0.01$ ,  $p < 0.001$ , respectively). In addition, caveolae-mediated endocytosis pathway inhibitor – filipin and genistein were observed to decrease the internalization of APT-NP by 80% and 63% ( $p < 0.01$ ). Furthermore, pre-added APT<sub>EDB</sub> peptide also competitively and significantly inhibited the cellular association of APT-NP ( $p < 0.01$ ).

### 3.4. Cell apoptosis assay

To examine whether the encapsulation of PTX in APT<sub>EDB</sub>-conjugated nanoparticles facilitate cell apoptosis, the Hoechst 33258 staining method was used for characterizing the PTX-induced apoptotic cell death. As shown in Fig. 5A, the nuclei of untreated HUVEC cells showed no evidence of segmentation and fragmentation after Hoechst 33258 staining. In contrast, the cell nuclei displayed unsharp borders and fragmentation after treated with the PTX formulations for 24 h. Compared with Taxol<sup>®</sup> and NP-PTX, APT-NP-PTX did induce more severe fragmentation of the cell nuclei.

For quantitative analysis, the Annexin-V/PI double staining assay was performed to determine the percentage of cell apoptosis.

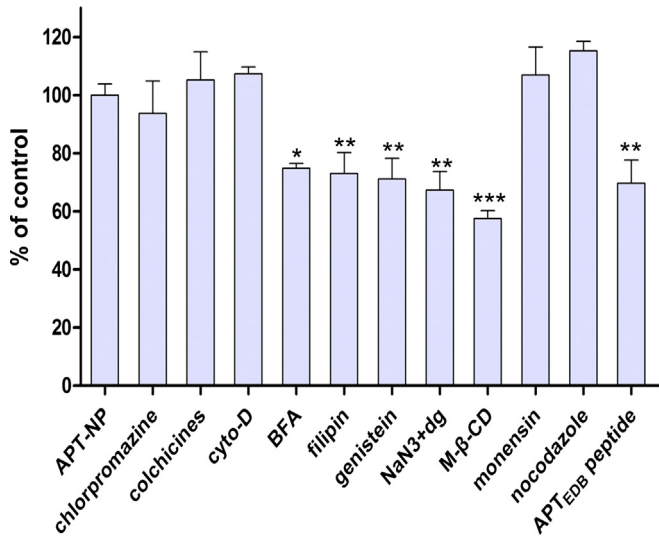


**Fig. 4.** Cellular uptake of coumarin-6-labeled APT-NP in HUVEC cells in the presence of different endocytosis inhibitors. Fluorescence intensity of coumarin-6 in the non-inhibited cells, representing the maximum internalized amount of coumarin-6-labeled APT-NP, was taken as control. \* $p < 0.05$ , \*\* $p < 0.01$ , \*\*\* $p < 0.001$  compared with control ( $n = 3$ ).

The rate of early and late apoptosis of HUVEC cells incubated 24 h with APT-NP-PTX were  $17.22 \pm 1.43\%$  and  $10.38 \pm 1.58\%$ , respectively. In contrast, Taxol<sup>®</sup> only caused  $7.25 \pm 1.23\%$  and  $5.23 \pm 0.72\%$  of early and late cell apoptosis, while NP-PTX caused  $9.91 \pm 1.65\%$  and  $9.13 \pm 1.18\%$ , respectively.

### 3.5. *In vitro* tube formation assay

We evaluated the effect of various paclitaxel formulations, Taxol<sup>®</sup>, NP-PTX and APT-NP-PTX on the formation of functional

tubes by plating HUVEC on Matrigel. As shown in Fig. 6, HUVEC cells subjected to DMEM treatment (blank control) formed extensive and enclosed tube networks. In contrast, Taxol<sup>®</sup> and NP-PTX displayed a relatively low activity in inhibiting tube formation, while APT-NP-PTX exhibited significant activity at drug concentrations of 1, 5 and 10 nM.

### 3.6. *In vivo* matrigel angiogenesis assay

*In vivo* matrigel plaque assay was also utilized to assess the anti-angiogenic effect of APT-NP-PTX. After the 7-day treatment with the different PTX formulations, Taxol<sup>®</sup>, NP-PTX and APT-NP-PTX, the mice were sacrificed and the sectioned matrigel plugs were stained with blood vessel marker CD31 to indicate the newly formed capillaries. As shown in Fig. 7, saline-treated mice showed substantial evidence of vascularization in the Matrigel plugs compared to those treated with PTX formulations. Consistent with the findings from the *in vitro* capillary-like network formation experiment, APT-NP-PTX led to a remarkably decrease in the number of blood vessels when compared with both Taxol<sup>®</sup> and NP-PTX.

### 3.7. Anti-proliferation assay

The anti-proliferative effect of different PTX formulations on U87MG cells was evaluated by CCK-8 assay. A strong growth inhibition of U87MG cells was found in all the PTX formulations, with IC<sub>50</sub> values for Taxol<sup>®</sup>, NP-PTX and APT-NP-PTX 90.74 nM, 74.58 nM and 23.32 nM, respectively (Fig. 8).

### 3.8. *In vivo* imaging

The active-tumor-targeting ability of APT-NP was evaluated non-invasively in subcutaneous U87MG tumor-bearing nude mice using DiR as the fluorescence probe. It is shown that DiR-labeled APT-NP accumulated more in the U87MG tumor tissue than DiR-labeled NP at 2 h after injection, and this pattern maintained for

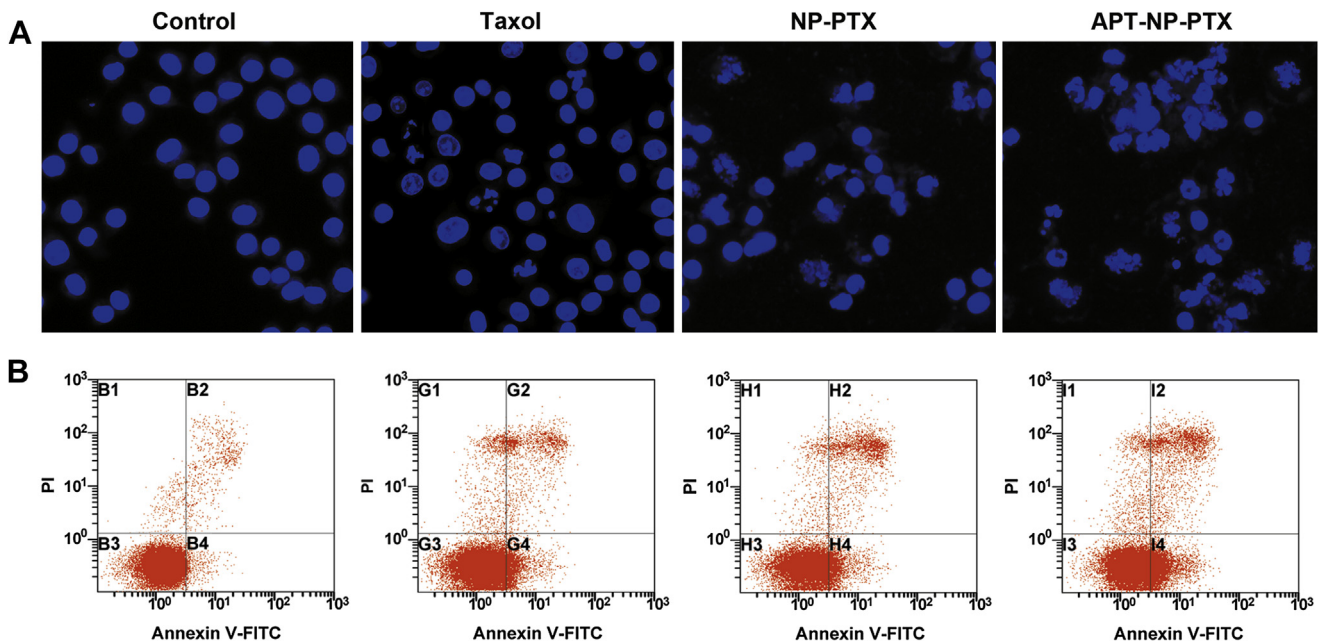


**Fig. 5.** Induction of apoptosis in HUVEC following 24 h incubation with various PTX formulations (PTX concentration 100 ng/ml). (A) Fluorescence micrographs of HUVEC cell nuclei labeled by Hoechst 33258. Original magnification: 20 $\times$ . (B) Flow cytometry analysis after staining with Annexin V-FITC and PI. HUVEC cells incubated with drug-free DMEM was served as the control.

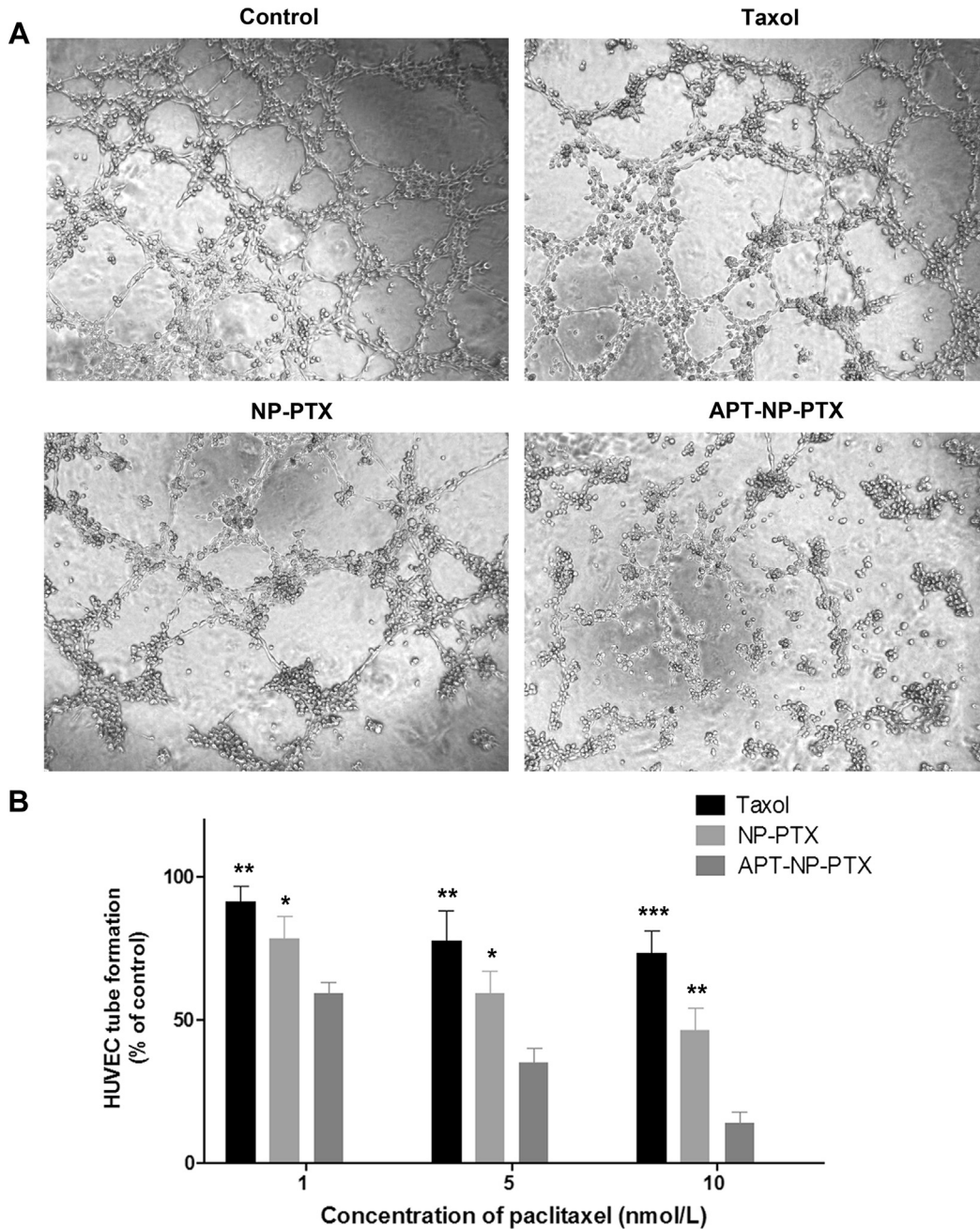


**Fig. 6.** Effect of various PTX formulation, Taxol<sup>®</sup>, NP-PTX and APT-NP-PTX on HUVEC tube formation. HUVEC cells incubated with drug-free DMEM served as the control. (A) The representative photographs of tube networks after treatment with various PTX formulations at the drug concentration of 10 nm. (B) The quantitative data for the HUVEC tube formation. Data were presented as the percentages of the control group, which was set at 100%. \* $p < 0.05$ , \*\* $p < 0.01$ , \*\*\* $p < 0.001$ , significantly different with that following the treatment with the same concentration of APT-NP-PTX.

the entire study (24 h after injection, Fig. 9A). Semi-quantitative analysis of region of interest (ROI) revealed that the tumor accumulation of APT-NP was 2.58-fold over that of NP (Fig. 9B).

### 3.9. In vivo tumor distribution

Three hours after administration, the APT-NP fluorescence was found highly accumulated at the tumor site, an appropriate amount of APT-NP was observed to extravasate and accumulate in the tumor parenchyma. In contrast, unmodified NP did not achieve significant accumulation in tumors (Fig. 10).

### 3.10. In vivo antitumor activity evaluation

Subcutaneous U87MG tumor xenograft model was also used to compare the antitumor activity of APT-NP-PTX with that of Taxol<sup>®</sup> and NP-PTX. Animals received saline was used as the negative control. Following the treatment, the tumor volume of the animals received the PTX formulations followed the order: APT-NP-PTX < NP-PTX < Taxol<sup>®</sup> < Saline. The final tumor volume of those mice treated with APT-NP-PTX was notably reduced (Fig. 11A, B). According to Fig. 11D, tumor weight in APT-NP-PTX group ( $0.07 \pm 0.03$  g) is significant lower than in saline ( $0.85 \pm 0.14$  g,

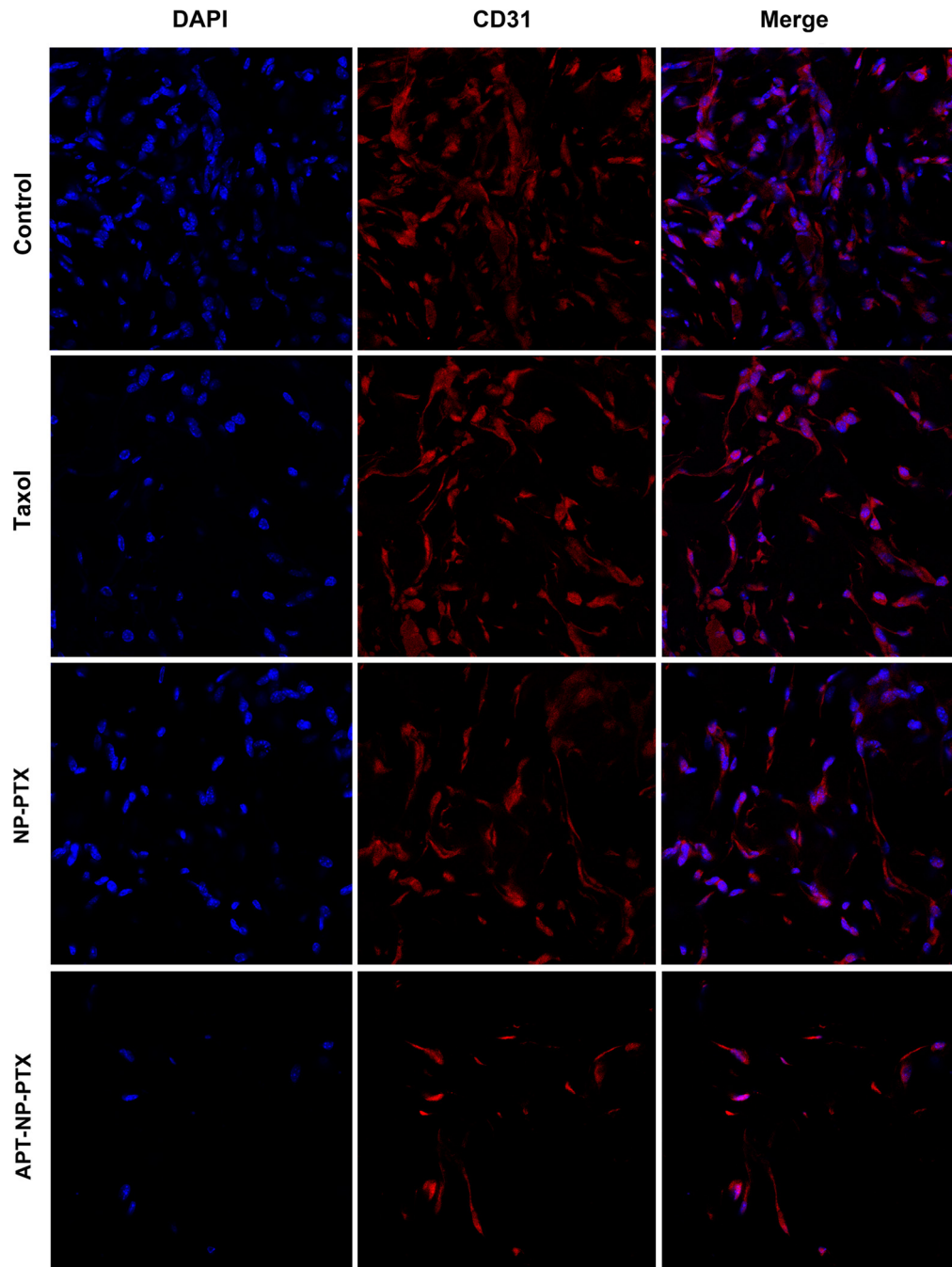


**Fig. 7.** Inhibition of *in vivo* Matrigel angiogenesis by PTX formulation, Taxol<sup>®</sup>, NP-PTX and APT-NP-PTX. Growth factor-reduced Matrigel containing bFGF were s.c. injected into BALB/c nude mice. The mice were treated with daily i.v. injections of Taxol<sup>®</sup>, NP-PTX and APT-NP-PTX (at a dose of 5 mg/kg PTX), or physiological saline as a control for 7 days. Matrigel plugs were removed 7 d later, subjected to frozen section and examined under a confocal microscope. Blood vessels were stained with anti-CD31 antibody (red), and nuclei were counterstained with DAPI (blue). Bars represent 50  $\mu$ m. (For interpretation of the references to color in this figure legend, the reader is referred to the web version of this article.)

$P < 0.001$ ), Taxol<sup>®</sup> ( $0.41 \pm 0.08$  g,  $P < 0.001$ ) and NP-PTX ( $0.28 \pm 0.06$  g,  $P < 0.01$ ) groups. In addition, the body weight of the APT-NP-PTX-treated animals was not different from that of the other groups (Fig. 11D).

### 3.11. Anti-glioma efficacy

The anti-glioma efficacy was also evaluated by measuring the survival time of those intracranial U87MG glioma bearing mice treated with the different PTX formulations every three days in two

weeks. As shown in Fig. 12, the medium survival time of the mice treated with saline, Taxol<sup>®</sup>, NP-PTX and APT-NP-PTX was 19, 24, 31, 41 days, respectively. APT-NP-PTX significantly prolonged animal survival time when compared with NP-PTX (\*\* $p < 0.01$ ), Taxol<sup>®</sup> (\*\* $p < 0.001$ ) and saline (\*\* $p < 0.001$ ).

## 4. Discussion

Angiogenesis is now established as one of the hallmarks of glioma, and is an essential prerequisite for glioma growth, progression

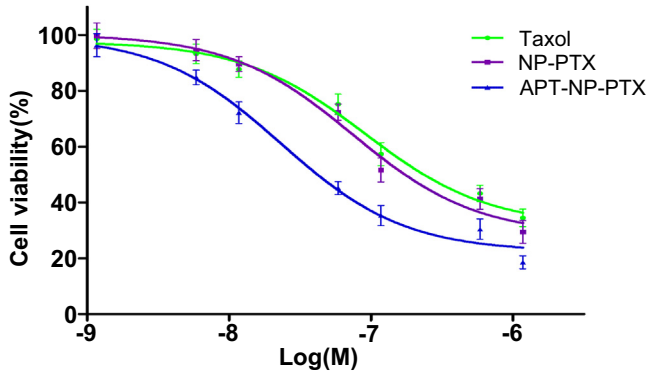


**Fig. 8.** *In vitro* cytotoxicity of various PTX formulations on U87MG glioma cells. The U87MG cells were plated at 5000 cells per well in the 96-well plate and cultured in growth medium for 24 h prior to the treatment with Taxol<sup>®</sup>, NP-PTX and APT-NP-PTX, respectively, for 72 h at 37 °C.

and metastasis [31]. However, the reactive resistance to the proapoptotic effect of chemotherapy as well as the enhanced metastatic and invasive potential of tumor cells largely limited the application of anti-angiogenic therapy for glioma treatment [32–35]. Therefore, tumor neovasculature and tumor cells dual-targeting chemotherapy is urgently needed to decrease the side

effect of anti-angiogenic therapy and also possesses the potential to be applied to a wide range of malignant tumors [36].

The identification of neovascular and tumor cellular markers and the isolation of high-affinity ligands are the most important issues in dual-targeting strategies [37]. EDB-containing fibronectin, which is highly expressed on the surface of both endothelial cells of tumor neovasculature and glioma cells, offers a suitable target for glioma drug delivery [38]. APT<sub>EDB</sub> is a small peptide with affinity to EDB at nanomolar range. Therefore, in this study, we developed a nanoparticulate DDS, APT<sub>EDB</sub> peptide-conjugated nanoparticles, which can target tumor neovasculature and glioma cells, and improve the anti-glioma efficacy of PTX.

In this study, PTX-loaded PEG-PLA nanoparticles were prepared through an emulsion/evaporation method, and APT<sub>EDB</sub> peptide was decorated to nanoparticles via a maleimide-mediated covalent binding procedure. The obtained APT-NP-PTX exhibited an average particle size of  $125.93 \pm 9.84$  nm. The modification of APT<sub>EDB</sub> on the surface of NP was verified by XPS analysis, which showed 0.87% nitrogen on the nanoparticle surface of APT-NP. Furthermore, *in vitro* release results showed that the decoration of APT<sub>EDB</sub> peptide did not change the release profile of the nanoparticles. From both NP-PTX and APT-NP-PTX, PTX release in plasma was slightly faster than that in PBS, which might be attributed to the presence of enzymes in the plasma [39].

Over-expression of EDB-containing fibronectin was found on the surface of endothelial cells of tumor neovasculature and glioma

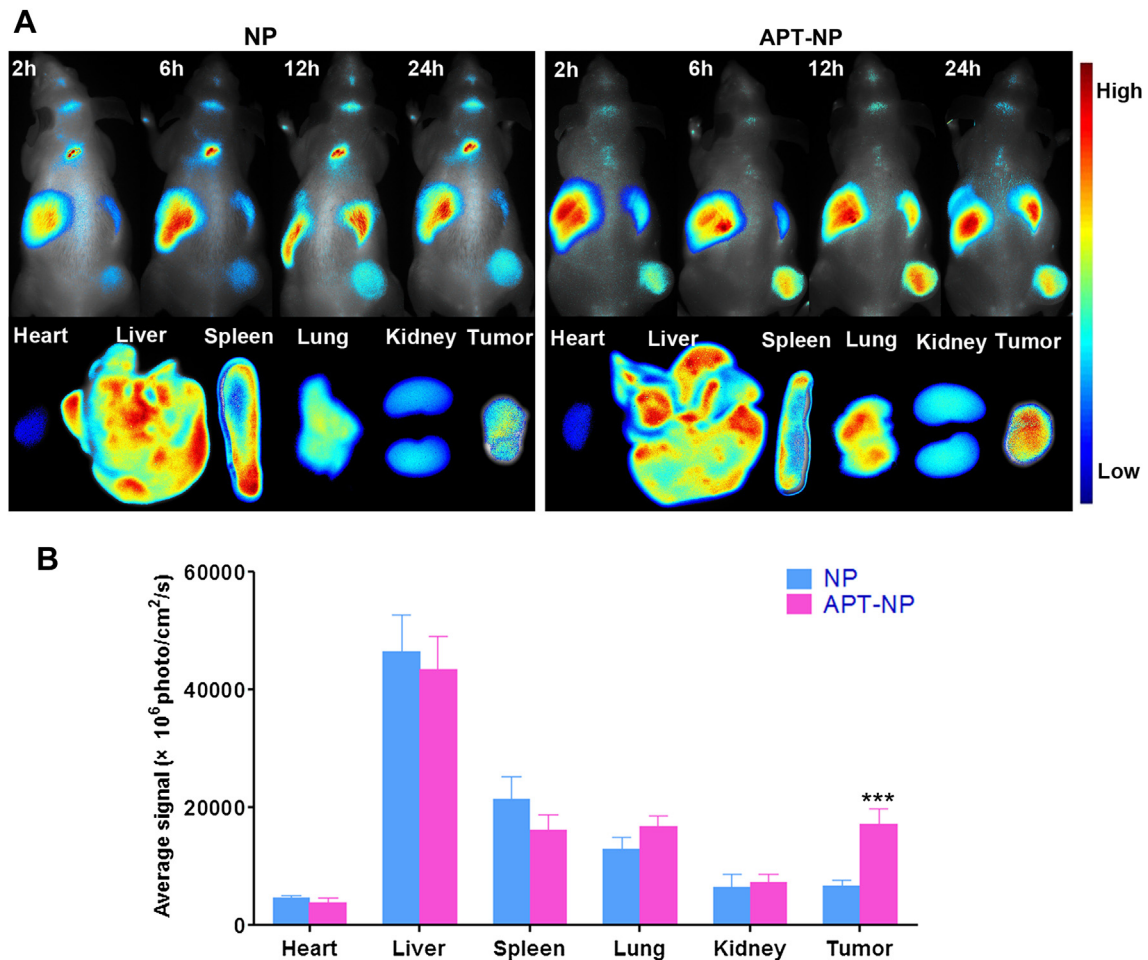


**Fig. 9.** (A) *In vivo* fluorescence imaging of subcutaneous U87MG tumor-bearing nude mice and the dissected organs after intravenous injection with DiR-labeled NP and APT-NP. (B) Semi-quantitative of intensity of different organs and tumor. The data are presented as the mean  $\pm$  SD ( $n = 3$ ). \*\*\* $P < 0.001$ , significantly higher than that of NP.

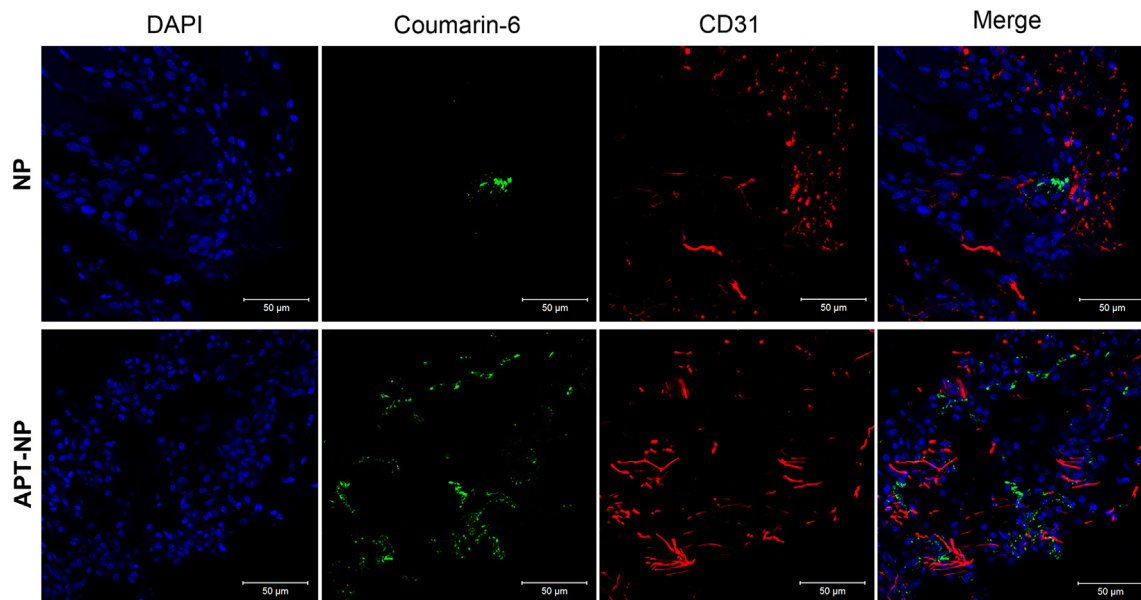


**Fig. 10.** Distribution of the coumarin-6-labeled NP and APT-NP in tumor tissue of subcutaneous xenografts bearing mice 3 h after i.v. administration. Frozen sections were examined under a confocal microscope. Blood vessels were visualized with anti-CD31 (red), nuclei were stained with DAPI (blue), while green was represented the NPs. Bars represent 50  $\mu\text{m}$ . (For interpretation of the references to color in this figure legend, the reader is referred to the web version of this article.)

cells, thus the nanoparticulate DDS functionalized with APT peptide would achieve a significant uptake in both cells. As shown in Figs. 2A and 3A, cellular uptake of PEG-PLA nanoparticles in HUVEC cells and U87MG cells was significantly enhanced following the surface conjugation with APT<sub>EDB</sub>, at each concentration point. A

time-, temperature- and concentration-dependant cellular association of APT-NP was observed (Fig. 2B,C, Fig. 3B,C), suggesting a process of active endocytosis. Taken the qualitative and quantitative results together, we claimed that APT-NP showed significant dual-targeting efficiency *in vitro*.

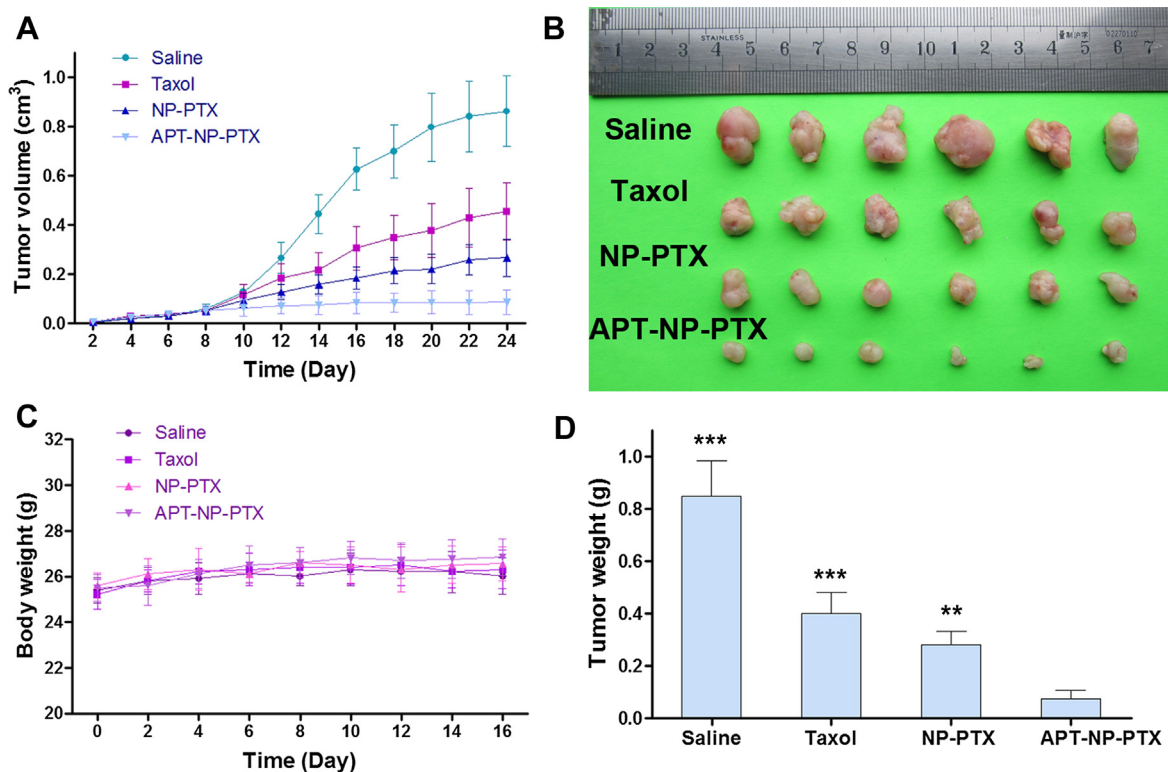


**Fig. 11.** *In vivo* antitumor activity of Taxol<sup>®</sup>, NP-PTX, APT-NP-PTX (PTX dose of 5 mg/kg) and physiological saline, respectively, after five consecutive injections (repeated every three days) at the dose of 5 mg/kg PTX. (A) Changes in tumor volumes from different PTX formulations. (B) Photographs of tumors from each tested group. (C) Changes in mice body weights over time. (D) The weights of excised tumor masses. Data represents mean  $\pm$  SD,  $n = 6$ . \*\* $p < 0.01$ , \*\*\* $p < 0.001$ , significantly different from that of the APT-NP-PTX group.

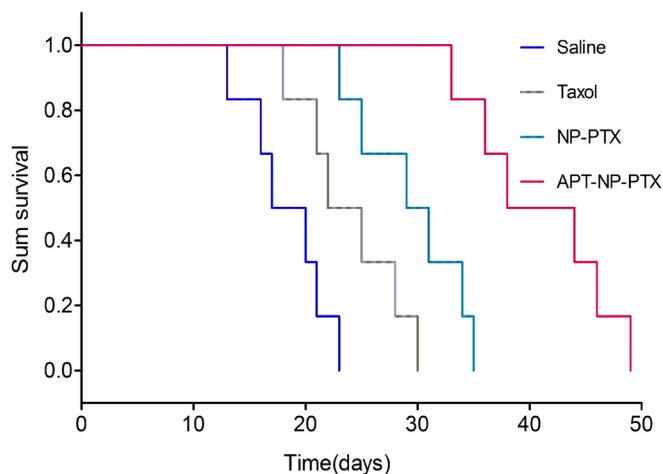


**Fig. 12.** Kaplan–Meier survival curve of mice bearing intracranial U87MG glioma treated with saline, Taxol<sup>®</sup>, NP-PTX and APT-NP-PTX every three days in two weeks at the PTX dose of 5 mg/kg ( $n = 6$ ).

To clearly identify the endocytosis pathways that involved in the cellular internalization of APT-NP, cellular association of the nanoparticles were performed in the presence of various endocytosis inhibitors [40]. It was found that filipin, genistein and NaN<sub>3</sub> significantly reduced the cellular uptake of APT-NP (Fig. 4), indicating that energy-dependent and caveolae-mediated endocytosis played an important role in the cellular uptake of APT-NP [41,42]. In the meanwhile, the cellular association of APT-NP was also inhibited by BFA and M- $\beta$ -CD, indicating that the endocytosis process in HUVEC cells was lipid raft-mediated and Golgi apparatus involved [43,44]. Furthermore, free APT<sub>E<sub>DB</sub></sub> peptide competitively reduced the cellular association of APT-NP, confirming the contribution of APT<sub>E<sub>DB</sub></sub> modification to the enhanced cellular uptake.

The improved cellular uptake led to the anticipated enhanced anti-angiogenic activity. The apoptosis analysis demonstrated that APT-NP-PTX induced more apoptosis in HUVEC cells (Fig. 5), which could be due to the higher cellular accumulation of PTX via the APT<sub>E<sub>DB</sub></sub> peptide-mediated endocytosis. To determine whether APT-NP-PTX could reduce the ability of HUVEC to form tube-like structures, we performed the tube formation assay in growth factor-reduced Matrigel *in vitro*, a widely accepted approach to measure the reorganization stage of angiogenesis [45]. APT-NP-PTX exhibited higher activity of inhibiting HUVEC tube formation than NP-PTX and Taxol<sup>®</sup> (Fig. 6), suggesting a potential for decreasing angiogenesis. To further confirm the anti-angiogenic effects of APT-NP-PTX *in vivo*, a Matrigel plug assay was performed. Consistent with the findings from the *in vitro* assay, a significant decrease in terms of capillary density and vessels numbers in the Matrigel plugs of those mice treated with APT-NP-PTX was observed (Fig. 7). These data together confirmed that the antiangiogenic ability of PTX was significantly improved following its encapsulation in APT-NP, which can be ascribed to the active cellular internalization mediated by the interaction between APT<sub>E<sub>DB</sub></sub> and EDB that specifically and highly expressed on the endothelial cells of neovasculature.

The improved cellular uptake in U87MG cells also resulted in an enhanced anti-proliferation effect. Significantly increased cytotoxicity was achieved for APT-NP-PTX (IC<sub>50</sub> 3.89 times lower than that of Taxol<sup>®</sup>, 3.19 times lower than that of NP-PTX), which we believed was also contributed by the enhanced cellular association of the nanoparticles following the modification with APT<sub>E<sub>DB</sub></sub>.

*In vivo* near-infrared (NIR) imaging experiments were performed to evaluate the solid tumor targeting effects of APT-NP in

nude mice bearing subcutaneous U87MG tumor xenografts. Accumulation of APT-NP in the tumor site was much higher than that of NP (Fig. 9), suggesting that a strong tumor targeting effect could be achieved by APT-NP. Furthermore, *in vivo* tumor distribution analysis revealed that only a small amount of unmodified NP could reach the tumor site through the EPR effect, but an obviously higher accumulation and wider distribution was achieved by APT-NP (Fig. 10). Moreover, an appropriate amount of APT-NP was observed to extravasate and accumulate in the tumor parenchyma, suggesting that our tumor neovasculature and tumor cells dual-targeting DDS might also facilitate extravascular transport of nanoparticles within the tumor.

To evaluate the antitumor activity of APT-NP-PTX *in vivo*, tumor-bearing nude mice were treated with PTX formulations every three days for five consecutive injections. As shown in Fig. 11, APT-NP-PTX exhibited the most powerful antitumor activity, which is believed to be contributed by the increased nanoparticle accumulation in tumor site as well as the enhanced anti-angiogenic and antitumor activity. Moreover, the enhanced antitumor efficacy of APT-NP-PTX was achieved without any accompanied toxicity as the body weight of APT-NP-PTX-treated animals were similar with that of other groups.

The anti-glioma efficiency of APT-NP-PTX was also evaluated in male Balb/c nude mice xenografted with U87MG glioma cells intracranially. As shown in Kaplan–Meier survival curve (Fig. 12), an enormous prolonged survival was achieved by those intracranial-U87MG-glioma-bearing mice treated with APT-NP-PTX (the medium survival time 41 days), significantly longer than those mice treated with NP-PTX (30 days,  $**p < 0.01$ ), Taxol<sup>®</sup> (24 days,  $***p < 0.001$ ) and saline (19 days,  $***p < 0.001$ ). Such improved anti-glioma efficiency of APT-NP-PTX could be very likely contributed by the increased dual-targeting efficiency and promoted anti-cancer drug accumulation at tumor site due to the APT<sub>E<sub>DB</sub></sub> modification.

## 5. Conclusion

We here developed a nanoparticulate DDS, PTX-loaded PEG-PLA nanoparticles conjugated with APT<sub>E<sub>DB</sub></sub> peptide for tumor neovasculature and tumor cells dual-targeting drug delivery. The resulted APT-NP exhibited significantly elevated cellular accumulation in HUVEC cells and U87MG cells, and improved the apoptosis-induction activity of PTX. The uptake of APT-NP in HUVEC cells was enhanced via energy-dependent, caveolae and lipid raft-mediated endocytosis. Anti-angiogenic activity of APT-NP-PTX was confirmed by *in vitro* tube formation assay and *in vivo* matrigel angiogenesis assay. *In vivo* near-infrared (NIR) imaging and *in vivo* tumor distribution showed that APT-NP displayed a much better tumor targeting and higher accumulation within the tumor. More importantly, APT-NP-PTX exhibited the most powerful antitumor activity without observable accompanied toxicity. Survival experiment further confirmed the improved anti-glioma efficacy of APT-NP-PTX. These findings indicated that APT<sub>E<sub>DB</sub></sub>-conjugated nanoparticles hold high potential for improving the anti-angiogenic and anti-glioma efficacy of the loaded cargoes.

## Acknowledgments

This work was supported by National Natural Science Foundation of China (81373353), National Key Basic Research Program (2013CB932500), Grants from Shanghai Science and Technology Committee (13NM1400500, 11430702200, 12nm0502000, 12ZR1416300), Program for New Century Excellent Talents in University (NCET-12-0130), Innovation Program of Shanghai Municipal Education Commission (12ZZ107) and FDUOP (Fudan's Undergraduate Research Opportunities Program, 14011).

## References

- [1] Remer S, Murphy ME. The challenges of long-term treatment outcomes in adults with malignant gliomas. *Clin J Oncol Nurs* 2004;8:368–76.
- [2] Chamberlain M. Evolving strategies: future treatment of glioblastoma. *Expert Rev Neurother* 2011;11:519–32.
- [3] Hu Q, Gu G, Liu Z, Jiang M, Kang T, Miao D, et al. F3 peptide-functionalized PEG-PLA nanoparticles co-administrated with tLyp-1 peptide for anti-glioma drug delivery. *Biomaterials* 2013;34:1135–45.
- [4] Beduneau A, Saulnier P, Benoit JP. Active targeting of brain tumors using nanocarriers. *Biomaterials* 2007;28:4947–67.
- [5] Weis SM, Cheresh DA. Tumor angiogenesis: molecular pathways and therapeutic targets. *Nat Med* 2011;17:1359–70.
- [6] Khasraw M, Ameratunga M, Grommes C. Bevacizumab for the treatment of high-grade glioma: an update after phase III trials. *Expert Opin Biol Ther* 2014;14:729–40.
- [7] Neri D, Bicknell R. Tumor vascular targeting. *Nat Rev Cancer* 2005;5:436–46.
- [8] Liu C, Zhang N. Emerging biotechnological strategies for non-viral anti-angiogenic gene therapy. *Angiogenesis* 2012;15:521–42.
- [9] Gordon MS, Mendelson DS, Kato G. Tumor angiogenesis and novel anti-angiogenic strategies. *Int J Cancer* 2010;126:1777–87.
- [10] Paez-Ribes M, Allen E, Hudock J, Takeda T, Okuyama H, Vinals F, et al. Anti-angiogenic therapy elicits malignant progression of tumors to increased local invasion and distant metastasis. *Cancer Cell* 2009;15:220–31.
- [11] Hu Q, Gao X, Kang T, Feng X, Jiang D, Tu Y, et al. CGKRK-modified nanoparticles for dual-targeting drug delivery to tumor cells and angiogenic blood vessels. *Biomaterials* 2013;34:9496–508.
- [12] Zhang B, Wang H, Liao Z, Wang Y, Hu Y, Yang J, et al. EGFP-EGF1-conjugated nanoparticles for targeting both neovascular and glioma cells in therapy of brain glioma. *Biomaterials* 2014;35:4133–45.
- [13] Rybak JN, Trachsel E, Scheuermann J, Neri D. Ligand-based vascular targeting of disease. *Chemmedchem* 2007;2:22–40.
- [14] Tarli L, Balza E, Viti F, Borsi L, Castellani P, Berndorff D, et al. A high-affinity human antibody that targets tumoral blood vessels. *Blood* 1999;94:192–8.
- [15] Nilsson F, Kosmehl H, Zardi L, Neri D. Targeted delivery of tissue factor to the ED-B domain of fibronectin, a marker of angiogenesis, mediates the infarction of solid tumors in mice. *Cancer Res* 2001;61:711–6.
- [16] Santimaria M, Moscatelli G, Viale GL, Giovannoni L, Neri G, Viti F, et al. Immunoscintigraphic detection of the ED-B domain of fibronectin, a marker of angiogenesis, in patients with cancer. *Clin Cancer Res* 2003;9:571–9.
- [17] Mariani G, Lasku A, Balza E, Gaggero B, Motta C, Di Luca L, et al. Tumor targeting potential of the monoclonal antibody BC-1 against oncofetal fibronectin in nude mice bearing human tumor implants. *Cancer* 1997;80:2378–84.
- [18] Sauer S, Erba PA, Petrini M, Menrad A, Giovannoni L, Grana C, et al. Expression of the oncofetal ED-B-containing fibronectin isoform in hematologic tumors enables ED-B-targeted 131I-L19SIP radioimmunotherapy in Hodgkin lymphoma patients. *Blood* 2009;113:2265–74.
- [19] Kim S, Kim D, Jung HH, Lee IH, Kim JI, Suh JY, et al. Bio-inspired design and potential biomedical applications of a novel class of high-affinity peptides. *Angew Chem Int Ed Engl* 2012;51:1890–4.
- [20] Saw PE, Kim S, Lee IH, Park J, Yu M, Lee JJ, et al. Aptide-conjugated liposome targeting tumor-associated fibronectin for glioma therapy. *J Mater Chem B* 2013;1:4723–6.
- [21] Allen TM. Ligand-targeted therapeutics in anticancer therapy. *Nat Rev Cancer* 2002;2:750–63.
- [22] Hu Q, Gao X, Gu G, Kang T, Tu Y, Liu Z, et al. Glioma therapy using tumor homing and penetrating peptide-functionalized PEG-PLA nanoparticles loaded with paclitaxel. *Biomaterials* 2013;34:5640–50.
- [23] Xia H, Gao X, Gu G, Liu Z, Hu Q, Tu Y, et al. Penetratin-functionalized PEG-PLA nanoparticles for brain drug delivery. *Int J Pharm* 2012;436:840–50.
- [24] Xia H, Gao X, Gu G, Liu Z, Zeng N, Hu Q, et al. Low molecular weight protamine-functionalized nanoparticles for drug delivery to the brain after intranasal administration. *Biomaterials* 2011;32:9888–98.
- [25] Gu G, Xia H, Hu Q, Liu Z, Jiang M, Kang T, et al. PEG-co-PCL nanoparticles modified with MMP-2/9 activatable low molecular weight protamine for enhanced targeted glioblastoma therapy. *Biomaterials* 2013;34:196–208.
- [26] Kang T, Gao X, Hu Q, Jiang D, Feng X, Zhang X, et al. iNGR-modified PEG-PLGA nanoparticles that recognize tumor vasculature and penetrate gliomas. *Biomaterials* 2014;35:4319–32.
- [27] Zeng N, Gao X, Hu Q, Song Q, Xia H, Liu Z, et al. Lipid-based liquid crystalline nanoparticles as oral drug delivery vehicles for poorly water-soluble drugs: cellular interaction and in vivo absorption. *Int J Nanomed* 2012;7:3703–18.
- [28] Yu DH, Lu Q, Xie J, Fang C, Chen HZ. Peptide-conjugated biodegradable nanoparticles as a carrier to target paclitaxel to tumor neovasculature. *Biomaterials* 2010;31:2278–92.
- [29] Christian S, Pilch J, Akerman ME, Porkka K, Laakkonen P, Ruoslahti E. Nucleolin expressed at the cell surface is a marker of endothelial cells in angiogenic blood vessels. *J Cell Biol* 2003;163:871–8.
- [30] Jiang X, Xin H, Gu J, Xu X, Xia W, Chen S, et al. Solid tumor penetration by integrin-mediated pegylated poly(trimethylene carbonate) nanoparticles loaded with paclitaxel. *Biomaterials* 2013;34:1739–46.
- [31] Kavitha CV, Agarwal C, Agarwal R, Deep G. Asiatic acid inhibits pro-angiogenic effects of VEGF and human gliomas in endothelial cell culture models. *PLoS One* 2011;6:e22745.
- [32] Kim JY, Shim X, Choi HW, Park J, Chung SW, Kim S, et al. Tumor vasculature targeting following co-delivery of heparin-taurocholate conjugate and suberoylanilide hydroxamic acid using cationic nanolipoplex. *Biomaterials* 2012;33:4424–30.
- [33] Morales AR, Yanez CO, Zhang Y, Wang X, Biswas S, Urakami T, et al. Small molecule fluorophore and copolymer RGD peptide conjugates for ex vivo two-photon fluorescence tumor vasculature imaging. *Biomaterials* 2012;33:8477–85.
- [34] Luo LM, Huang Y, Zhao BX, Zhao X, Duan Y, Du R, et al. Anti-tumor and anti-angiogenic effect of metronomic cyclic NGR-modified liposomes containing paclitaxel. *Biomaterials* 2013;34:1102–14.
- [35] Yu DH, Ban FQ, Zhao M, Lu Q, Lovell JF, Bai F, et al. The use of nanoparticulate delivery systems in metronomic chemotherapy. *Biomaterials* 2013;34:3925–37.
- [36] Arap W, Pasqualini R, Ruoslahti E. Cancer treatment by targeted drug delivery to tumor vasculature in a mouse model. *Science* 1998;279:377–80.
- [37] Cheng Z, Al Zaki A, Hui JZ, Muzykantor VR, Tsourkas A. Multifunctional nanoparticles: cost versus benefit of adding targeting and imaging capabilities. *Science* 2012;338:903–10.
- [38] Kaspar M, Zardi L, Neri D. Fibronectin as target for tumor therapy. *Int J Cancer* 2006;118:1331–9.
- [39] Guo J, Gao X, Su L, Xia H, Gu G, Pang Z, et al. Aptamer-functionalized PEG-PLGA nanoparticles for enhanced anti-glioma drug delivery. *Biomaterials* 2011;32:8010–20.
- [40] Gu G, Gao X, Hu Q, Kang T, Liu Z, Jiang M, et al. The influence of the penetrating peptide iRGD on the effect of paclitaxel-loaded MT1-AF7p-conjugated nanoparticles on glioma cells. *Biomaterials* 2013;34:5138–48.
- [41] Aoki T, Nomura R, Fujimoto T. Tyrosine phosphorylation of caveolin-1 in the endothelium. *Exp Cell Res* 1999;253:629–36.
- [42] Mo Y, Lim LY. Mechanistic study of the uptake of wheat germ agglutinin-conjugated PLGA nanoparticles by A549 cells. *J Pharm Sci* 2004;93:20–8.
- [43] Vercauteren D, Vandenbroucke RE, Jones AT, Rejman J, Demeester J, De Smedt SC, et al. The use of inhibitors to study endocytic pathways of gene carriers: optimization and pitfalls. *Mol Ther* 2010;18:561–9.
- [44] Jiang S, Rhee SW, Gleeson PA, Storrie B. Capacity of the golgi apparatus for cargo transport prior to complete assembly. *Mol Biol Cell* 2006;17:4105–17.
- [45] Akhtar N, Dickerson EB, Auerbach R. The sponge/Matrigel angiogenesis assay. *Angiogenesis* 2002;5:75–80.